INSTITUTE OF PHYSICS PUBLISHING PLASMA PHYSICS AND CONTROLLED FUSION

Plasma Phys. Control. Fusion **46** (2004) 723–750 PII: S0741-3335(04)67415-X

Study of Type III ELMs in JET

R Sartori[1], G Saibene[1], L D Horton[2], M Becoulet[3], R Budny[4], D Borba[5], A Chankin[2], G D Conway[2], G Cordey[6], D McDonald[6], K Guenther[6], M G von Hellermann[7], Yu Igithkanov[8], A Loarte[1], P J Lomas[6], O Pogutse[6] and J Rapp[9]

[1] EFDA Close Support Unit, Garching, 2 Boltzmannstrasse, Garching (DE), Germany
[2] Association Euratom-IPP, MPI fur Plasmaphysik, 2 Boltzmannstrasse, Garching (DE), Germany
[3] Association Euratom-CEA, CE Cadarache, F-13108 St Paul-lez-Durance, CEDEX, France
[4] PPPL, Princeton University, PO Box 451, Princeton, NJ 08543, USA
[5] Associacao EURATOM/IST, Centro de Fusao Nuclear, 1096 Lisbon, CODEX, Portugal
[6] EURATOM-UKAEA Fusion Association, Culham Science Centre, Abingdon, OX14 3DB, UK
[7] FOM-Rijnhuizen, Ass. Euratom-FOM, TEC, PO Box 1207, 3430 BE Nieuwegein, The Netherlands
[8] Max-Planck-Institute for Plasma Physics, Teilinstitut Greifswald, EURATOM Ass., D-17491, Greifswald, Germany
[9] EFDA Close Support Unit, Culham, Abingdon OX14 3DB, UK

Received 11 August 2003
Published 26 March 2004
Online at stacks.iop.org/PPCF/46/723
DOI: 10.1088/0741-3335/46/5/002

Abstract

This paper presents the results of JET experiments aimed at studying the operational space of plasmas with a Type III ELMy edge, in terms of both local and global plasma parameters. In JET, the Type III ELMy regime has a wide operational space in the pedestal n_e–T_e diagram, and Type III ELMs are observed in standard ELMy H-modes as well as in plasmas with an internal transport barrier (ITB). The transition from an H-mode with Type III ELMs to a steady state Type I ELMy H-mode requires a minimum loss power, P_{TypeI}. P_{TypeI} decreases with increasing plasma triangularity. In the pedestal n_e–T_e diagram, the critical pedestal temperature for the transition to Type I ELMs is found to be inversely proportional to the pedestal density ($T_{\mathrm{crit}} \propto 1/n$) at a low density. In contrast, at a high density, T_{crit}, does not depend strongly on density. In the density range where $T_{\mathrm{crit}} \propto 1/n$, the critical power required for the transition to Type I ELMs decreases with increasing density. Experimental results are presented suggesting a common mechanism for Type III ELMs at low and high collisionality. A single model for the critical temperature for the transition from Type III to Type I ELMs, based on the resistive interchange instability with magnetic flutter, fits well the density and toroidal field dependence of the JET experimental data. On the other hand, this model fails to describe the variation of the Type III n_e–T_e operational space with isotopic mass and q_{95}. Other results are instead suggestive of a different physics for Type III ELMs. At low collisionality, plasma current ramp

experiments indicate a role of the edge current in determining the transition from Type III to Type I ELMs, while at high collisionality, a model based on resistive ballooning instability well reproduces, in term of a critical density, the experimentally observed q_{95} dependence of the transition from Type I to Type III ELMs. Experimental evidence common to Type III ELMs in standard ELMy H-modes and in plasmas with ITBs indicates that they are driven by the same instability.

(Some figures in this article are in colour only in the electronic version)

1. Introduction

Type III ELMy H-modes are commonly observed in all divertor tokamaks. In comparison with the Type I ELMy regime, these ELMy H-modes are characterized by small high frequency ELMs and by reduced energy confinement (10–30%). The Type III ELMy regime represents a limit to the operational space of Type I ELMs. In fact, at high density, the transition from Type I to Type III ELMs limits the density achievable with good confinement. Moreover, the transition to Type III ELMs also defines the minimum power below which Type I ELMs are no more observed.

In plasmas with an internal transport barrier (ITB), the benefit (in terms of the divertor transient power load) of a Type III ELMy edge is combined with the transport reduction in the core plasma. In JET, this regime is achieved at relatively low pedestal densities compared with the Greenwald density and the pedestal collisionality of these plasmas is low ($\nu^* < 5 \times 10^{-2}$). Under these conditions, keeping the edge in the Type III ELMy regime and avoiding a transition to Type I ELMs is an issue since large Type I ELMs can interact with the ITB, causing its 'erosion' [1].

The reference scenario for $Q = 10$ inductive operation in ITER is a standard ELMy H-mode with Type I ELMs. This operating point is relatively close to the Type III operational boundary [2]. Therefore, a study of the operational space of Type III ELMs and its scaling with machine and plasma parameters is important for the control and/or the avoidance of these ELMs.

This paper reports the results of experiments carried out in JET to study the operational space of Type III ELMs. Those experiments were carried out in the standard ELMy H-modes regimes, but the results will be compared with the findings for plasmas with an ITB. The operational space of Type III ELMs is studied in terms of global plasma parameters such as input power, plasma density, toroidal field, and plasma triangularity (these findings are reported in sections 2 and 3) as well as in terms of the pedestal parameters n_e and T_e (section 4). The dedicated experiments described in this paper were carried out with the JET Mark II Gas Box (GB) divertor. The results of previous JET experiments with the Mark IIA divertor [3] are consistent, both in terms of the behaviour of global and local parameters, with the results described here, but one significant difference is also observed. A comparison between the GB and Mark IIA results is briefly discussed in section 5. In section 6, the JET experimental data are compared with some theoretical models for Type III ELMs. The results of this comparison are discussed highlighting common features and differences between Type III ELMs with and without an ITB and between Type III ELMs at high and low pedestal collisionality. Finally, section 7 is dedicated to an analysis of the energy confinement of Type III ELMy H-modes and to discussing briefly the reasons and extent of the confinement degradation with respect to the Type I ELMy regime.

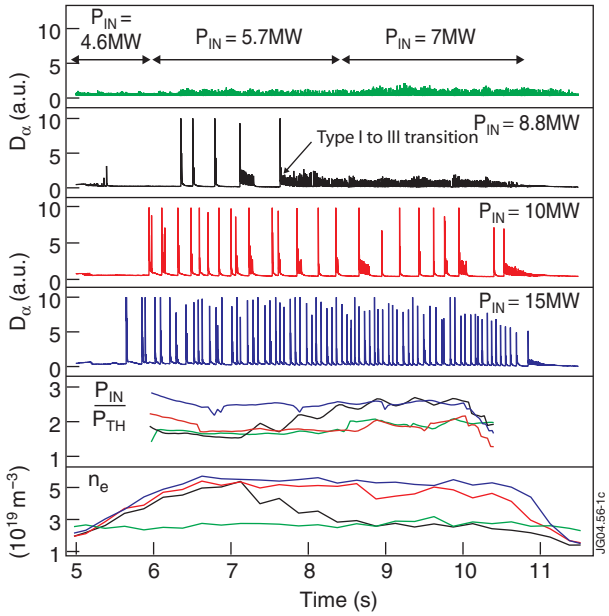

Figure 1. Power scan at 2.5 MA/2.5 T for a low δ plasma, $\delta \cong 0.22$, with the strike points on the vertical plate of the divertor. The first four boxes show the time evolution of the D_α signal, for discharges with increasing input power. The last two boxes show the evolution of the ratio of the input power to the predicted L–H threshold power, P_{IN}/P_{L-H}, and of the line averaged density, n_e, as the power is increased (#45526, 46228, 46227, 47541).

2. The power threshold for Type I ELMs

ELMy H-modes with Type III ELMs are observed at low powers above the predicted L–H threshold power, $P_{L-H} = 0.45 n_e^{0.75} B_t R^2$ [4]. According to the definition given in [5, 6], in H-modes with Type III ELMs the ELM frequency, f_{ELM}, decreases with increasing input power. Figures 1 and 2 illustrate the typical features of a power scan in JET, for neutral beam heated ELMy H-modes without any external gas fuelling. In this example, the plasma current, I_p, was 2.5 MA, the toroidal field, B_t, was 2.4 T ($q_{95} \cong 3$). The plasma average triangularity, δ, was $\cong$0.22.

In the power scan of figure 1 the input power, P_{IN}, is increased in steps, starting from P_{IN} just above P_{L-H}. At the lowest input powers ($P_{IN} \leqslant 7$ MW in figure 1) the plasma is in the Type III ELMy regime, which is characterized by high frequency ELMs with low D_α amplitude. At a slightly higher input power ($P_{IN} = 8.8$ MW in figure 1), the plasma might access the Type I ELM regime and sometimes maintain it for several energy confinement times, but permanent (relative to the heating pulse length) or cyclic transitions to the Type III ELM regime are observed. One such 'permanent' transition to Type III ELMs is shown in figure 1 (second box): the discharge with 8.8 MW neutral beam injection (NBI) has a period of Type I ELMs, which is followed by a transition to the Type III ELMy regime. This transition is accompanied by a large decrease in density and stored energy. At higher P_{IN} (10 MW, again in figure 1), a steady state Type I ELMy H-mode is achieved. 'Steady state' means, in this context, that the ELM type, the average diamagnetic stored energy, $\langle W_{DIA} \rangle$ (average over the ELM period), and the average plasma density are constant for the entire duration of the additional heating period. Under these conditions, the input power is equal to the average loss power, $\langle P_{loss} \rangle = P_{IN} - \langle dW_{DIA}/dt \rangle$.

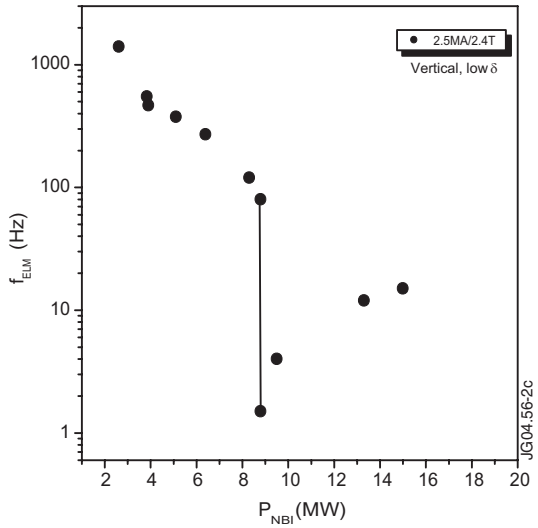

Figure 2. Power scan at 2.5 MA/2.5 T: ELM frequency versus power. The ELM frequency decreases with increasing NBI power for Type III ELMs, and it increases with power for Type I ELMs. The plasma with a transition from Type I to Type III ELMs is characterized by a double value of f_{ELM}.

In figure 2, the ELM repetition frequency, f_{ELM}, is plotted as a function of input power for the discharges of figure 1 and some additional discharges with the same plasma parameters. For P_{IN} less than $\cong$8 MW, f_{ELM} decreases with increasing P_{IN} (Type III ELMs), while for P_{IN} greater than $\cong$10 MW, f_{ELM} increases with input power (Type I ELMs). The plasma discharge with a transition from Type I to Type III is characterized, in the plot of f_{ELM} versus power, by two values of f_{ELM} for a given input power. The Type I ELM frequency of this plasma corresponds to the minimum of the Type I ELM frequency versus power (figure 2). In other words, Type I ELMy H-modes with minimum Type I ELM frequency are difficult to achieve in steady state. According to the general behaviour of the ELM type and ELM frequency versus power illustrated in figures 1 and 2, one can define 'power threshold for Type I ELMs', P_{TypeI}, as the lowest input power, P_{IN}, necessary to maintain in a steady state (as defined above) an ELMy H-mode with Type I ELMs. ($P_{\mathrm{TypeI}} \cong 10$ MW in the example of figures 1 and 2.)

Figure 3 illustrates that long additional heating pulse duration (long compared with the energy confinement time) and small increments in P_{IN} (small compared with the threshold power) are important for the determination of P_{TypeI}. Figure 3 shows the D_α race for two power scans in 2 MA/2 T plasma and with different plasma triangularities: $\delta \cong 0.25$ and $\delta \cong 0.33$. For these power scans, the steps in power were smaller than the ones in the example of figures 1 and 2, and the heating pulse duration was longer (8 s as opposed to 5 s). As indicated by the vertical line in figure 3, with 5 s of additional heating, the estimated power required to maintain Type I ELMs for the entire duration of the heating pulse would have been $\cong$30% lower. Figure 3 also shows that, as P_{IN} is increased, the transitions from Type I to Type III become cyclic, i.e. Type I ELMs are recovered at constant P_{IN}, and the total period with Type III ELMs becomes shorter. In fact, for example, the discharge with 5.9 MW ($\delta \cong 0.25$) is in the Type I ELMy regime only for 8% of the pulse duration, as opposed to the discharge with 7.6 MW NBI, which has Type I ELMs for 65% of the pulse duration. In summary, steady state Type III ELMs are observed at low powers above the L–H threshold power and steady state Type I ELMy H-modes are only observed above a critical power, P_{TypeI}. There is an

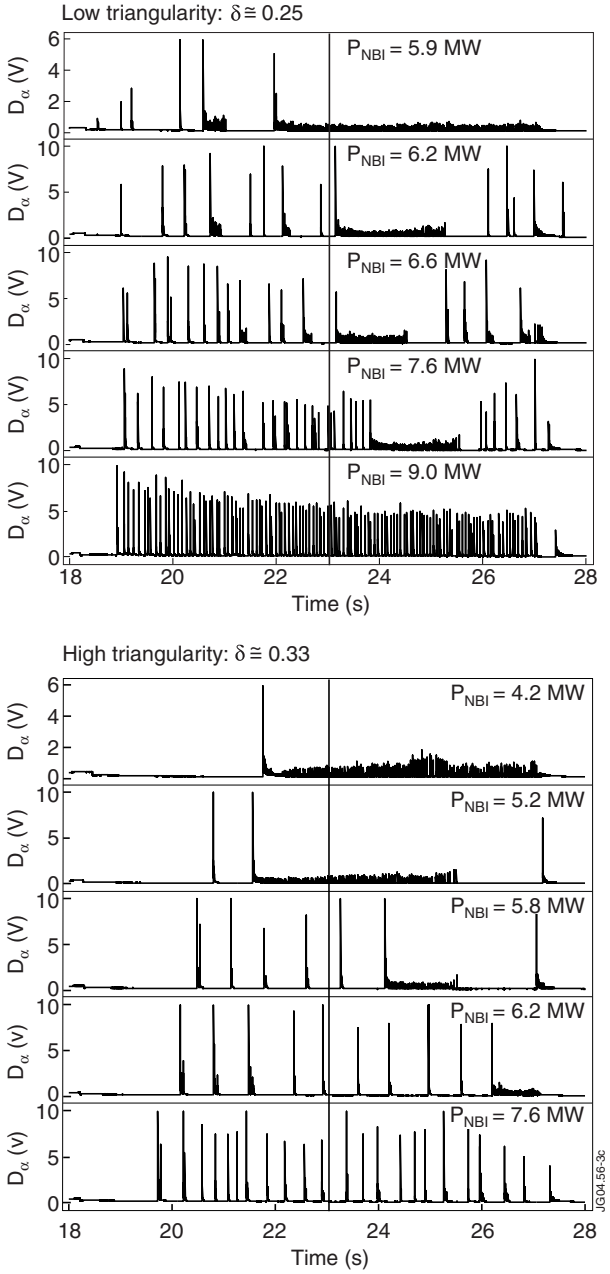

Figure 3. Divertor D_α traces for a power scan at 2.0 MA/2.0 T for a low triangularity plasma, upper figure, and high triangularity plasmas, lower figure (both with the strike points on the vertical divertor target). The vertical line marks a 5 s additional heating duration. Note that the duration of the initial phase with Type I ELMs increases with increasing P_{IN}.

intermediate range of power where phases with Type I and Type III ELMs coexist. In this range of power, the duration of the phases with Type III ELMs decreases with increasing P_{IN}.

Results from previous experiment carried out with the Mark IIA divertor [3] have already suggested that P_{TypeI} can be expressed empirically as a multiple of the predicted L–H threshold

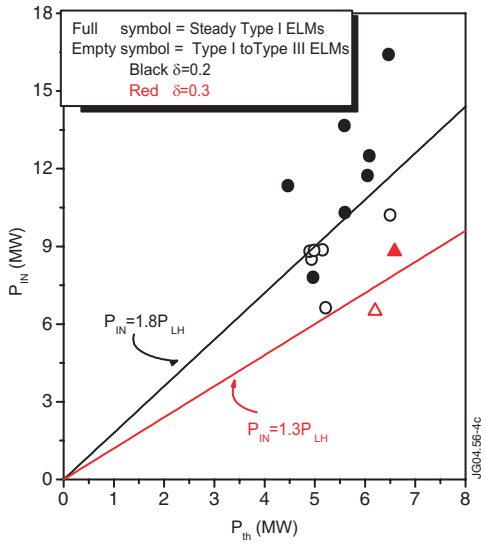

Figure 4. Power required to maintain Type I ELMs in a steady state, derived from a P_{IN}, B_{t}, and I_{p} scan with the JET GB divertor. Full symbols, steady H-modes with Type I ELMs; empty symbols, H-modes with a transition from the Type I to the Type III regime.

power, $P_{\mathrm{L–H}}$, or, in other words, that the parametric dependence of P_{TypeI} on n_{e} and B_{t} might be similar to the one of the L–H threshold power. A dedicated experiment to study the proportionality between $P_{\mathrm{L–H}}$ and P_{TypeI} was carried out with the JET Mark II GB divertor [7]. The results of this experiment are summarized in figure 4. In the experiment, power scans were carried out with NBI in plasmas with different I_{p} and B_{t} and at a fixed triangularity, $\delta \cong 0.25$. In a Type I ELMy H-mode with NBI, there is a minimum density that can be achieved. This density, called the 'natural' density, is the steady state density achieved without external gas fuelling, as in all the experiments described above. At low triangularity, $\delta \cong 0.25$, the natural density is $\cong$50% of the Greenwald density limit, n_{G}. As a consequence of the proportionality between the natural density and I_{p}, the predicted L–H threshold power increases with I_{p}. In the experiment summarized in figure 4, I_{p} was varied from 2 to 3 MA (2, 2.5, and 3 MA) at a B_{t} value of 2.4 T, and a power scan was carried out for each value of I_{p}. Similarly, at $I_{\mathrm{p}} = 2.5$ MA, P_{IN} was varied in plasmas with B_{t} increased to 3 T. In figure 4 the input power and predicted threshold power of steady state H-modes with Type I ELMs are compared with the same quantities in the initial Type I ELMy phase of plasmas where cyclic or permanent transitions to the Type III ELM regime are observed. As shown in the figure, the results of this experiment confirm the previous findings that an H-mode with Type I ELMs at low triangularity can be maintained in a steady state when the input power is about twice the predicted L–H threshold power: $P_{\mathrm{TypeI}} \cong 2P_{\mathrm{L–H}}$.

In this experiment I_{p} and n_{e} are not independent variables. Therefore, the proportionality of P_{TypeI} with $P_{\mathrm{L–H}}$ could be due to either an I_{p} or n_{e} dependence. Separate experiments [8] have shown that the L–H threshold power does not depend on I_{p}. The observed proportionality between P_{TypeI} and $P_{\mathrm{L–H}}$ suggests that P_{TypeI} too depends on density rather than on I_{p}. The result of this experiment on the proportionality between $P_{\mathrm{L–H}}$ and P_{TypeI} is consistent with the inverse mass dependence of both the L–H threshold power [9] and the power required for the transition to the Type I ELMy regime [9, 10]. The multiplication factor between P_{TypeI} and $P_{\mathrm{L–H}}$ exhibits some day-to-day variation ($\approx\pm$20% in GB, for a similar additional heating

pulse duration), suggesting a dependence not yet quantified on additional variables, generally referred to as an 'effect of vessel conditioning'.

Although the proportionality between P_{TypeI} and $P_{\mathrm{L–H}}$ is a useful global empirical scaling, figure 1 already shows that this scaling does not give a complete picture of the experimental results. In fact, the time evolution of the ratio $P_{\mathrm{IN}}/P_{\mathrm{L–H}}$ that follows the transition from Type I to Type III ELMs seems to be in contradiction with the picture of a simple proportionality between P_{TypeI} and $P_{\mathrm{L–H}}$ (figure 1; plasma with $P_{\mathrm{IN}} = 8.8\,\mathrm{MW}$, black traces). As shown in figure 1, a large decrease in plasma density is observed at the transition from the Type I to the Type III ELMy regime. As the density decreases, so does the predicted $P_{\mathrm{L–H}}(\propto n^{0.75})$, and the ratio $P_{\mathrm{IN}}/P_{\mathrm{L–H}}$ increases to values greater than 2. As a consequence, the H-mode should in principle recover the Type I ELMy behaviour. Figure 1 shows that this is not the case. It will be shown in section 4 that this apparent contradiction might be explained in terms of local variables and could also be related to the deviation of the L–H threshold power, at low density, from the predicted density scaling.

3. The effect of plasma triangularity on the power threshold for Type I ELMs

ELMy H-modes with different triangularity have different steady state parameters. In particular, the natural density increases with δ, being 60–70% of n_{G} for $\delta \cong 0.3$–0.4 [11], compared with 50% at $\delta \cong 0.2$. Moreover, the ELM frequency decreases with increasing δ. The higher natural density at high δ implies, at fixed input power, a lower margin above the L–H threshold power than at low δ. As a consequence, from the proportionality between P_{TypeI} and $P_{\mathrm{L–H}}$, one would expect that high triangularity plasmas would require higher powers for steady state Type I ELMs. On the contrary, the results of experiments with the Mark IIA divertor have already suggested that P_{TypeI} could be lower at high δ values than at low δ values. The variation of P_{TypeI} with δ was investigated in detail with the GB JET divertor [12]. The experiment was carried out at 2 MA/2 T, using NBI heating, with plasma triangularity values of 0.25 and 0.33. In JET the L–H power threshold was found to vary with divertor geometry [8]. In order to avoid any change in the L–H power threshold, the X-point height and strike point position were kept the same for the plasma configurations at $\delta = 0.25$ and 0.33. This was achieved by varying only δ_{upper} to change the plasma average triangularity, $\delta = (\delta_{\mathrm{upper}} + \delta_{\mathrm{lower}})/2$.

The D_α traces for some of the discharges in this experiment are shown in figure 3. In the power scan at $\delta = 0.33$, P_{TypeI} is 7.6 MW, compared with the 9 MW necessary to maintain Type I ELMs at $\delta = 0.25$. The experiment shows that the power threshold for Type I ELMs decreases with increasing δ. A similar result, but with a different $I_{\mathrm{p}}/B_{\mathrm{t}}$ combination (2.5 MA/2.4 T), is shown in figure 4, where for similar $P_{\mathrm{L–H}}$, P_{TypeI} is reduce by $\cong$30% at higher δ.

Although in these steady H-mode plasmas the average stored energy is constant, W is not constant on the timescale of the ELM period: on this timescale the loss power is reduced by the power required to re-heat the plasma between ELMs ($P_{\mathrm{loss}} = P_{\mathrm{IN}} - \mathrm{d}W_{\mathrm{DIA}}/\mathrm{d}t$). For similar plasma parameters, the ELM frequency decreases for increasing δ, and $\mathrm{d}W_{\mathrm{DIA}}/\mathrm{d}t$ between ELMs (approximated here as $\Delta W_{\mathrm{DIA}}/\Delta t$), is also lower for the high δ plasmas. Therefore, the loss power required for steady state Type I ELMs could in principle be similar at high and low δ values since both P_{IN} and $\mathrm{d}W_{\mathrm{DIA}}/\mathrm{d}t$ decrease with increasing δ. What is observed is instead that the minimum P_{loss} necessary for a steady state Type I ELMy H-mode is lower at a high δ value and the minimum power to the separatrix ($P_{\mathrm{loss}} - P_{\mathrm{rad(bulk)}}$) is also lower. These observations indicate that the lower P_{TypeI} at a high δ value is not related to the variation of the ELM frequency with δ.

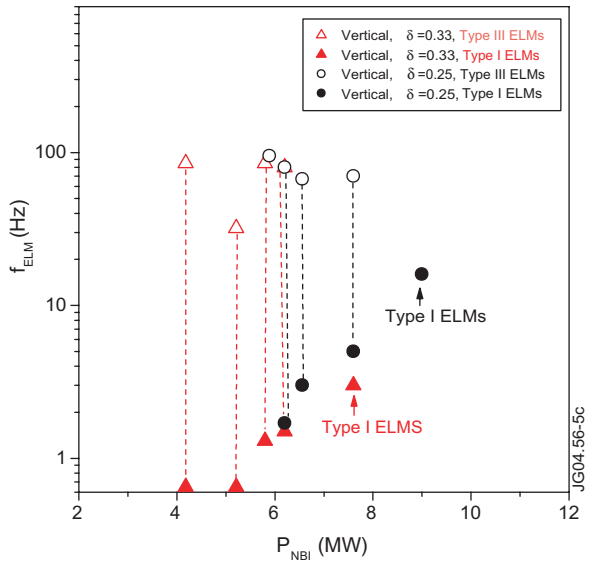

Figure 5. ELM frequency versus NBI power for the power scans at low and high δ values of figure 3. The Type I ELM frequency for the two high δ plasma at the lowest powers is only indicative due to the irregular ELM behaviour at low powers.

Figure 5 shows the ELM frequency as a function of the NBI input power for the high and low triangularity power scans of figure 3. The dotted lines indicate discharges that have periods both of Type I and of Type III ELMs, i.e. a double value of f_{ELM} for a given P_{IN}. The interval of power where this mixed ELM behaviour is observed gives an indication of the extent of the input power range where steady state plasmas with Type I ELMs are not achievable and of the possible error in the determination of P_{TypeI} due to the short pulse length.

In JET high density ELMy H-modes, it has been shown [13] that the power required to access a regime of good confinement at high density (mixed Type I-II ELMs, [14]) decreases with higher plasma triangularity. Therefore, the reduction in the power threshold for Type I ELMs with triangularity is observed in ELMy H-modes over the entire density range.

4. Local parameters—H-mode operational space

4.1. Observation of Type III ELMs at low and high pedestal density values

In this paper we refer to the Type III ELMs described in the previous sections as 'low density Type III ELMs'. In fact, in those low power Type III ELMy H-modes with no external gas fuelling the normalized density is typically only 25–30% of n_{G}. At high densities and higher input powers, a transition to Type III ELMy H-modes typically occurs when, at constant P_{IN}, the density of an H-mode with Type I ELMs is increased by gas fuelling [11, 15]. Therefore, from an operational point of view, low density Type III ELMs are observed in plasmas with no external fuelling at low input powers above the L–H threshold power. The transition to the Type I ELMy regime is obtained by increasing P_{IN} and thus the margin above $P_{\mathrm{L–H}}$. At high densities, the back transition from Type I ELMs to Type III ELMs occurs when the margin over $P_{\mathrm{L–H}}$ is decreased by increasing the density, at constant and relatively high input powers. As with low density Type III ELMs, the repetition frequency of high density Type III ELMs decreases with increasing $P_{\mathrm{IN}}-P_{\mathrm{rad}}$ [11].

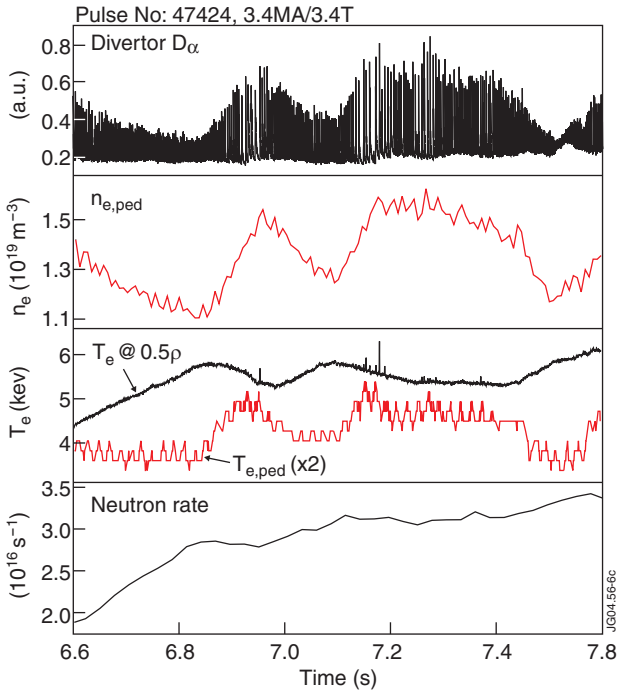

Figure 6. Time traces of divertor D_α, pedestal density, T_e at mid-radius (inside ITB) and at the pedestal, and neutron production rate, for #47424, with ITB and ETB. A correlation between the barrier strength (third box, showing the pedestal temperature and the temperature at mid-radius) and the frequency and amplitude of the ELMs is seen, as described in [1]. When the frequency of the ELMs decreases, both the absolute central temperature and the difference between the central and pedestal temperature decrease, indicating a decrease in the temperature gradient inside the plasma.

At low densities, in H-mode plasmas where a transition from the Type I to the Type III ELMy regime occurs (minimum of Type I ELM frequency), as well as in steady state Type I ELMy plasmas with input power just above P_{TypeI}, a 'compound' structure is often observed in the D_α trace after the Type I ELM crash (see figure 1). Type I ELMs with these characteristics are often called 'compound ELMs' in JET. In plasmas with compound ELMs, the large D_α spike of the Type I ELM is followed by a short period of more frequent ELMs with a lower D_α amplitude. These frequent ELMs have a D_α signature similar to that of Type III ELMs. Moreover, the density and stored energy behaviour that follow the Type I ELM crash are similar to those at the transition from Type I to Type III ELMs. Therefore we assume here that compound ELMs are very short periods of Type III ELMs that follow a Type I ELM, although the power dependence of f_{ELM} is difficult to verify since compound ELMs occur in a narrow power range and non-stationary conditions.

High frequency, low amplitude ELMs with a D_α signature similar to that of Type III ELMs are also observed in discharges with a simultaneous ITB [16] and H-mode edge transport barrier. The frequency and amplitude of these ELMs is often anti-correlated with the ITB strength [1] (as shown in figure 6). Those low amplitude ELMs are observed in plasmas with ITBs with an input power much higher than P_{TypeI} for standard ELMy H-modes but lower than the power required for Type I ELMs in the same regime [1, 17]. As in standard Type I ELMy H-modes, in ITB plasmas D–T operation reduces the additional heating power required for the transition

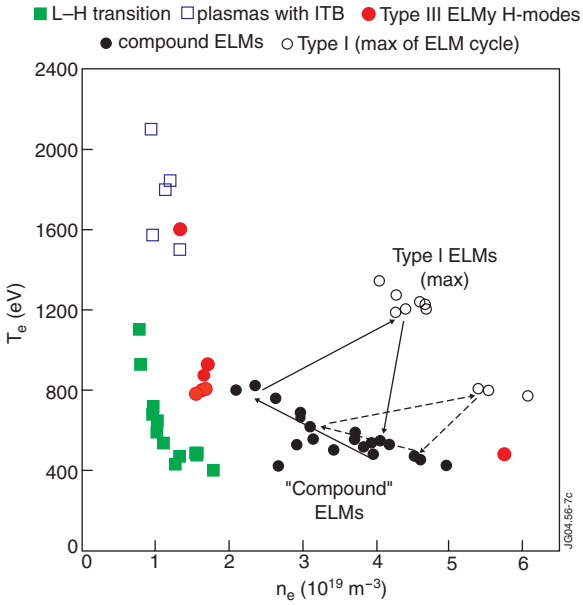

Figure 7. Pedestal n_e–T_e diagram for low triangularity plasmas at 2.5 MA/2.4 T [7] (the plasmas with ITB have B_t from 2.4 to 2.6 T. The arrows indicate the ELM cycle for a Type I ELM crash followed by compound ELMs.)

from those small ELMs to Type I ELMs [9, 10] and a lower power is required for Type I ELMs at higher plasma triangularity [19].

Although the power dependence of the ELM frequency of those low amplitude ELMs in plasmas with an ITB has not been studied in detail, we assume they are Type III ELMs on the basis of the similarities in the D_α signature.

The four categories of Type III ELMs (high and low density Type III ELMs, compound ELMs, and small ELMs of ITB plasmas) are observed in different regimes (H-modes with and without ITB) and span a very large density range: from very low densities, $n_e/n_G < 0.5$, for ITB plasmas, up to densities at, or approaching the Greenwald limit. Given the similarities highlighted before, we compare here the pedestal parameters for these four categories of ELMs. A comparison is shown in figure 7.

Figure 7 figure shows the pedestal electron temperature, T_e, from the ECE heterodyne radiometer, as a function of the electron line average density, n_e, given by the outermost channel ($R = 3.75$ m, $\rho \cong 0.95$) of the FIR interferometer, for plasmas at 2.5 MA/2.4 T (the plasmas with ITB have B_t from 2.4 to 2.6 T) with low triangularity ($\delta \cong 0.22$–0.25) and strike points on the vertical divertor plates or on the corner of the divertor, near the throat of the divertor cryo-pump. T_e is taken at the position of the top of the pedestal. For H-modes with Type I ELMs and for Type III ELMy H-modes at high density, the density profiles are relatively flat, and so the density at 3.75 m can be taken as the pedestal density. For Type III ELMy H-modes at low densities, where the density profile are more peaked (see section 7), taking n_e at 3.75 m may overestimate somewhat the pedestal density. As shown in figure 7, Type III ELMs of plasmas with an ITB have the lowest pedestal density and the highest pedestal temperature. In the ELMy H-mode regime, the lowest pedestal density (and highest $T_e \cong 1600$ eV) is achieved for a plasma configuration with the strike points in the corner of the divertor. This configuration is optimized for pumping by the JET divertor cryo-pump. As shown in figure 7, due to the

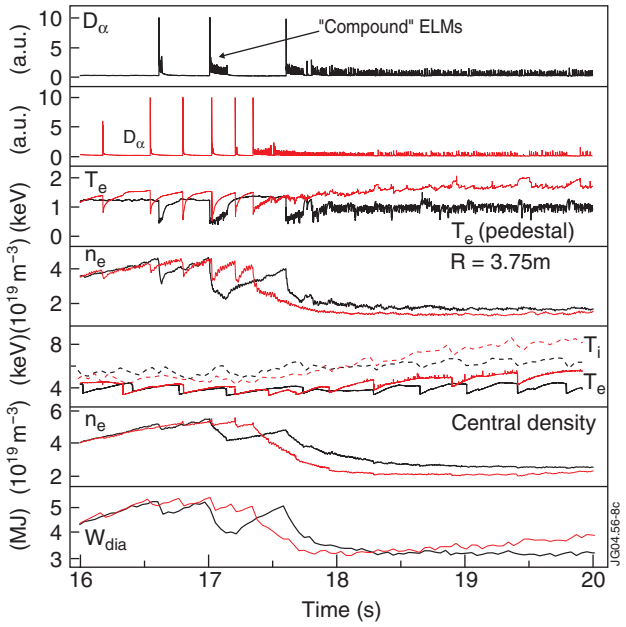

Figure 8. Evolution of the pedestal and core n and T_e and core T_i at the transition from the Type I to the Type III ELMs regime at a low density; 2.5 MA/2.4 T, $P_{IN} = 9$ MW. Pulse 46246 (black), strike points on the vertical target; pulse 46241 (red), strike points in the corner.

increased divertor pumping, the corner configuration produces a standard H-mode with very low pedestal densities and pedestal temperatures in the same range as the T_e of plasmas with an ITB. Therefore, the pedestal parameters for low density Type III ELMs, which follow the expected inverse power dependence of f_{ELM}, overlap the n_e–T_e operational space of the small ELMs of ITB plasmas, giving confidence to the assumption that the latter are indeed also Type III ELMs. The continuous and dotted arrows in figure 7 describe the n_e–T_e trajectory of the pedestal top with Type I ELMs that are followed by compound ELMs. The drop in pedestal temperature associated with the Type I ELM crash is followed by the evolution of the pedestal parameters towards lower n_e and higher T_e values during the phase of compound ELMs. Compound ELMs can be seen as temporary transitions to the Type III regime, from which the confinement is then recovered. Their trajectory in the n_e–T_e space is in the region of intermediate densities and temperatures.

Figure 7 shows the pedestal n_e and T_e for high density ELMy H-modes at a high pedestal density and low temperature, where the transition to the Type III ELMy regime is induced by external strong gas fuelling.

To further illustrate the behaviour of the pedestal parameters at the transition from Type I to Type III ELMs at a low density and the differences between the corner and vertical configurations, figure 8 shows the time evolution of D_α, the pedestal and core n_e and T_e, core T_i, and the diamagnetic stored energy, W_{DIA}, for two low density plasma, at the transition from Type I to Type III ELMs.

The red traces belong to an H-mode with a plasma configuration with the strike points in the corner of the divertor, while the black traces are for a plasma with the strike points on the vertical plate of the divertor. The figure shows, for both plasmas, the large drop in both pedestal and core density at the transition from Type I to Type III ELMs. The pedestal (and core) T_e with Type III ELMs is instead equal to the average value during the Type I ELMy phase for

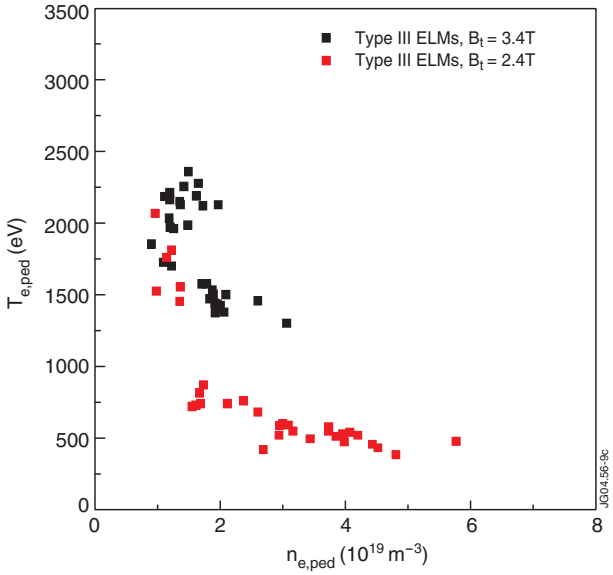

Figure 9. Pedestal n_e–T_e diagram for 2.5 MA/2.4–2.6 T and 3.3–3.6 MA/3.4 T Type III ELMy H-modes. n_e from the FIR interferometer outermost channel and T_e from the ECE heterodyne radiometer.

the vertical configuration. In the corner configuration (lower pedestal n_e), the pedestal T_e with Type III ELMs can be higher than the maximum T_e reached in the Type I ELM cycle. The core T_i shows a similar time evolution at the transition from Type I to Type III ELMs and is higher than T_e in those low density plasmas. The figure also shows the large drop in plasma stored energy at the transition to Type III ELMs. Figure 8 also illustrates that with compound ELMs the behaviour of the pedestal n_e and T_e are similar to what is observed at the final transition to Type III ELMs, but the drop in density is smaller.

The density dependence of the critical temperature for Type III ELMs is similar to the one of the critical temperature for the L–H transition [8]. The experimental n_e–T_e at the L–H transition is also shown in figure 7. Experiments with the GB divertor [8] have shown that, below a critical density, the critical temperature for the L–H transition increases with decreasing density. For densities below this critical density, the measured P_{L-H} increases (or remains constant) for decreasing density, so that deviations from the L–H threshold power predicted by the scaling are observed.

Considering together all the observations of Type III ELMs summarized in figure 7, one can see from figure 9 (where the same data of figure 7 are plotted in red) that the pedestal plasma temperature, in the Type III ELM regime, does not depend strongly on density at high n_e values and increases with decreasing density at low n_e values. For most of the points of figure 9, the temperature plotted is a 'critical temperature', that is, any increase in T_e will produce a transition to Type I ELMs. In fact, for the Type III ELMy H-modes in figure 7 (red circles), it has been experimentally verified that a small step-up in power during the Type III ELMy phase does produce a transition to Type I ELMs. For the ITB plasmas, one can see in figure 6 that there can be various transitions from Type III ELMs back to Type I ELMs within the same discharge. The temperature plotted in figures 7 and 9 for those plasmas is the T_e just before such transitions. In the high density ELMy H-modes, either a step-up in power or a decrease in density triggers the transition to Type I ELMs. One could consider also the T_e

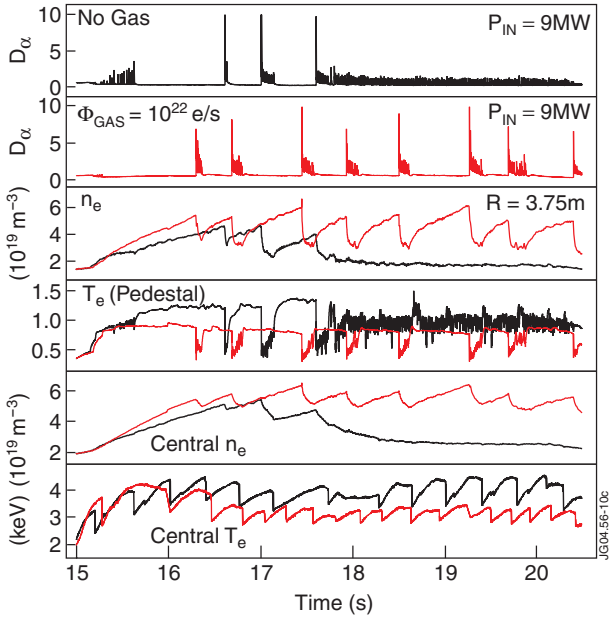

Figure 10. Effect of gas puff; 2.5 MA/2.4 T, $P_{IN} = 9$ MW. 46246, no gas; 46248, with gas fuelling. The pedestal density is given by the outermost channel of the FIR interferometer (see comments on page 11).

during compound ELMs to be 'critical' since at higher power the compound ELM behaviour disappears.

Figure 9 also show a set of low density Type III ELMy H-mode data for plasmas at $B_t = 3.4$ T. This set of data includes n_e–T_e for compound ELMs. For this higher B_t (and I_p), high density data are not available. The scatter of the data is larger at 3.4 T than at lower fields. This larger scatter is at least partially due to the fact that, since fewer dedicated experiments were done at 3.4 T and hence fewer data are available at this toroidal field, the 3.4 T data represent more an existence domain for Type III ELMs in the n_e–T_e space than a critical boundary for T_e. Figure 9 shows that, while the density dependence of the Type III ELMs critical temperature is similar at low and high B_t values, T_e is larger at higher toroidal field values.

4.2. Dependence of the Type I ELM transition on pedestal density

Since the critical temperature for the transition from Type III to Type I ELMs increases at low density in a manner similar to that of the L–H critical temperature, one could conceive that, below a certain density, P_{TypeI} might also increase. Experimentally, one indeed finds that increasing the density of a low density Type III discharge reduces the power threshold for Type I ELMs. Already in the Mark IIA experiments we have observed that with reduced divertor pumping (and no external fuelling), resulting in higher pedestal n_e and lower T_e, it was possible to maintain Type I ELMs at lower powers [3].

Figure 10 shows the results of an experiment carried out in the GB divertor to test the dependence of P_{TypeI} on density at a low density. With identical P_{IN}, the discharge with a constant external fuelling of 10^{22} atoms s^{-1} is in the Type I ELM regime (marginally, because compound ELMs are observed), while the discharge with no fuelling collapses to that of the

lower confinement, Type III regime. In a manner similar to that of the reduced divertor pumping, the effect of the external fuelling is to increase both the edge and core n_e and reduce edge and core T_e. The trajectory of the compound ELMs of the plasma with gas fuelling is indicated in figure 7 by the dotted arrows, while the compound ELMs with no gas fuelling are shown, in the same figure, by the continuous arrow. A possible interpretation of the result of this experiment is that, for the lower density plasmas with no external fuelling, a higher temperature (i.e. higher power) is required for the transition from Type III to Type I ELMs since $T \propto 1/n$. In other words, at a low density, P_{TypeI} increases as the density decreases. The behaviour of P_{TypeI} and of the L–H threshold power at a low density could explain why the decrease in density and consequent increase in the predicted $P_{\mathrm{IN}}/P_{\mathrm{L–H}}$ that accompanies the transition to Type III ELMs (as shown in figure 1 and discussed in the first section) does not lead to the plasma recovering the Type I ELM behaviour. In the density range where the critical temperature for the transition from Type III to Type I ELMs is $\propto 1/n$, an increase in input power as well as an increase in density triggers a transition to the Type I ELMy regime.

5. Type III ELMs at low densities: comparison between the Mark IIA and Mark II GB divertors

The results discussed in the previous sessions, in particular the correlation between P_{TypeI} and $P_{\mathrm{L–H}}$ and the dependence of P_{TypeI} on density, B_t, and triangularity, were also found with the JET Mark IIA divertor [20]. Nevertheless, one significant difference is observed in the behaviour of low collisionality plasmas with the Mark IIA and GB divertors: at low densities, Mark IIA plasmas with P_{IN} slightly below P_{TypeI} remained in the L-mode. The results of the Mark IIA experiments will be summarized briefly in this section, and the possible reason for the absence of Type III ELMs at low collisionality with the Mark IIA divertor will also be discussed. With the Mark IIA JET divertor [20], extensive experiments were carried out with ELMy H-modes in deuterium at high plasma current ($3.5\,\mathrm{MA} \leqslant I_p \leqslant 5\,\mathrm{MA}$) and low δ ($\delta \cong 0.22$) values, in preparation for the JET D–T experiment [3]. Those experiments highlighted the limits in operational space for Type I ELMy H-modes at low triangularity, when operating at high currents and toroidal fields. One of the main restrictions for these experiments was the limited additional heating power available in JET: the available power was marginal/not sufficient to achieve H-modes with Type I ELMs at high I_p values. In high I_p plasmas, a transition to the L-mode regime, sometimes preceded by a brief period transition to Type III ELMs, was observed [21]. Although the occurrence of the L-mode transition was associated with operation with input powers, P_{IN}, too close to the H-mode threshold power, $P_{\mathrm{L–H}}$ [21], this transition occurred at relatively high input powers, up to about twice the L–H predicted threshold power. The correlation between the power required to maintain Type I ELMs and the L–H threshold was confirmed by the D–T experiment, where a wider operational space in Type I ELMs for high I_p plasmas was found, consistent with the inverse isotope mass dependence of the L–H threshold.

Figure 11 shows a comparison between the transition to the L-mode observed with the Mark IIA divertor at a high I_p value and the transition to the Type III ELMy regime with the GB divertor.

Most of the results described in the previous sections are common for ELMy H-modes with the Mark IIA and the Mark II GB divertor. Similar to the behaviour with the GB divertor, at input power just below P_{TypeI} the Mark IIA plasma could access the Type I ELMy regime, but transitions (cyclic or permanent) to a lower confinement mode (L-mode) were observed. The experiments in Mark IIA and GB used a different plasma magnetic configuration: the divertor strike points were on the horizontal divertor target in Mark IIA, while with the GB divertor, due

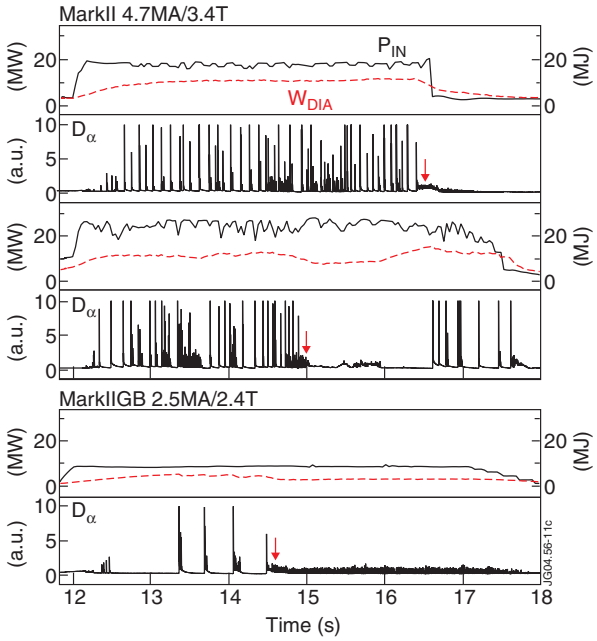

Figure 11. The loss of confinement with the Mark IIA and GB divertors. #38880/38891 at 4.7 MA/3.4 T (Mark IIA) and 46229 at 2.5 MA/2.4 T (GB).

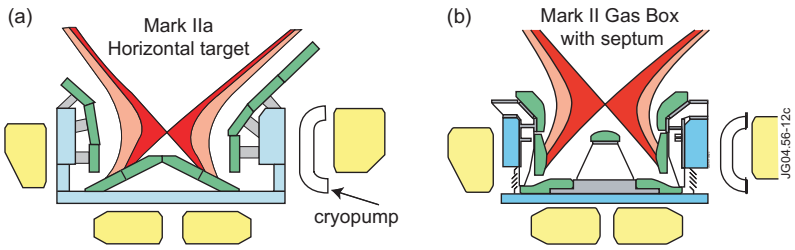

Figure 12. The Mark IIA divertor (left) and the GB divertor (right). With the Mark IIA divertor, plasma configurations with the stike points on the horizontal (as in the figure) and vertical targets were possible. With the GB divertor, only configurations with the strike points on the vertical target or on the corner of the divertor are possible.

to the presence of the divertor septum, only configurations with the strike points on the vertical divertor target, or on the corner of the divertor, were possible (see figure 12). The measured H-mode power threshold for GB discharges with the strike points on the vertical target is higher than the H-mode power threshold for Mark IIA plasmas with the strike points on the horizontal target [8, 18]. Consistently, we find that higher power is required to maintain a Type I ELMy H-mode in a steady state in GB than was required in Mark IIA. In summary, while both the measured $P_{\mathrm{L-H}}$ and P_{TypeI} values were lower with the Mark IIA divertor, a transition from the Type I ELMy regime to L-mode was observed in Mark IIA at $P_{\mathrm{IN}} < P_{\mathrm{TypeI}}$. These two findings are in apparent contradiction. Most probably, what prevented the Mark IIA plasmas from maintaining an H-mode pedestal with Type III ELMs was the presence of a $n = 1$ MHD instability localized in the pedestal region [21].

This mode was always present during the L-mode phase (but not during the short Type III phases, if they were present), and it disappeared if the plasma made a transition back to

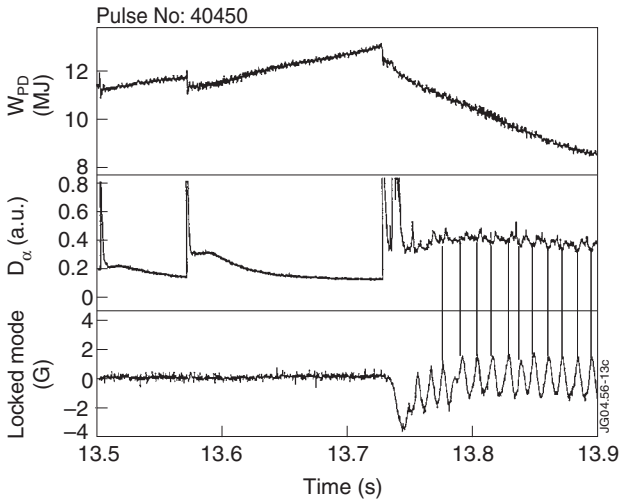

Figure 13. The $n = 1$ mode signature as seen by the locked mode detector and D_α signal.

Type I ELMs in the same discharge. As reported in [21], the mode had a low frequency of the order of 100 Hz. This $n = 1$ mode was localized in the plasma edge, since $m > q_{95}$. In some cases, as the one shown in figure 13, the mode and the D_α signature were correlated. The nature of this instability as well as the reason why it is not present with the GB divertor is not known. The mode was clearly unstable for the lowest collisionality and stable at the power levels required for a steady state H-mode with Type I ELMs. Similar to the ELMy H-mode behaviour, plasmas with an ITB also had an L-mode edge with the Mark IIA divertor but an H-mode edge with the GB divertor [22].

6. Discussion and comparison of the experimental data with models

As described in section 3, the pedestal n_e–T_e of Type III ELMy H-modes in JET covers a wide range of density and temperature. At a low density, the pedestal T_e increases with decreasing pedestal density approximately as $1/n$ and increases with increasing toroidal field (see figure 9). At a high density the pedestal temperature is independent of density or the density dependence is very weak. The Type III ELMy data of figure 9 have been compared with the model proposed by Pogutse and Igitkhanov [23, 24]. According to this model, Type III ELMs are caused by resistive interchange instability where the driver is provided by magnetic flutter (RIF). When the radial electric field just inside the separatrix becomes sufficiently strong, it can stabilize the RIF. This condition gives the upper boundary for Type III ELMs in the n_e–T_e diagram as

$$\beta' \lambda' \rho'^{-1/3} > c_\tau^2 q^2,$$

where $\beta' = (M_i/m_e)^{3/2}\beta_n s^2/q$ and $\rho' = \rho/R$ is the normalized toroidal Larmor radius. $\lambda' = 1/\nu'$, where ν' is the dimensionless flutter frequency: $\nu' = c_F s(1+c_\nu^2\{qR/\lambda_e\}^2)^{1/2}$ [23, 24].

From this condition, the asymptotic scaling for the critical temperature for the transition from Type III to Type I ELMs can be derived for two ranges of collisionality:

$$T_{0\mathrm{cirt}} \propto (c_\tau^2 c_F c_\nu)^{6/17} \frac{q^{24/17} R^{4/17} B_0^{10/17}}{A^{8/17} s^{12/17}} \qquad \text{for } \lambda_e < c_\nu q R,$$

$$T_{0\mathrm{cirt}} \propto (c_\tau^2 c_F)^{6/5} \frac{q^{18/5} R^{-2/5} B_0^2}{A^{8/5} s^{12/5} n_0^{6/5}} \qquad \text{for } \lambda_e > c_\nu q R,$$

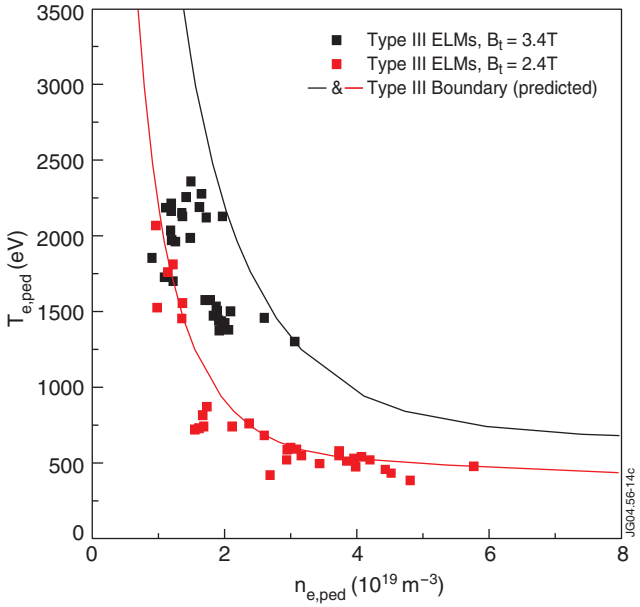

Figure 14. Pedestal n_e–T_e diagram for 2.5 MA/2.4–2.6 T and 3.3–3.6 MA/3.4 T discharges. n_e from the FIR interferometer outermost channel and T_e from the ECE heterodyne radiometer. The data are compared with the critical temperature (or upper boundary) for Type III ELMs predicted by the model of [23] and [24].

where c_τ, c_F, and c_ν are fitting constants, n_e and T_e are taken at the top of the H-mode pedestal, and the safety factor, q, and shear, s, are taken as q_{95} and s_{95}. The model prediction of the critical temperature, T_{0cirt}, is compared with the JET data at $B_t = 2.4$ and 3.4 T in figure 14 (same set of data as figure 9). The deuterium plasmas at $B_t = 2.4$ and 3.4 T have low shear ($s_{95} \cong 3$) and similar q_{95} (q_{95} from $\cong$3 to $\cong$3.3). For both toroidal fields, the data include ELMy H-mode plasmas and plasmas with simultaneous ITBs and ETBs. The fit coefficients have been adjusted to fit the 2.4 T data, and the same coefficients were used then for the 3.4 T data and for the analysis presented in the following figures. Although the coefficients used here for the Type III ELM boundary are different from the ones used in ([24], see also [25, 26]) to fit the Type III ELM boundary for ASDEX-U, DIII-D, and Alcator C-MOD, using the same coefficients given in [24] to fit the JET data results in little difference in the predicted curves for T_{0cirt}. This analysis shows that there is good agreement between the model and the experimental data. In particular, the model reproduces the strong increase in the critical temperature of Type III ELMs with B_t that is observed at low collisionality.

In figure 15, the same set of data of figure 14 is shown with the additional L–H transition data at 2.4 T, already presented in figure 7. The data for the electron temperature just before the L–H transition (at the position where the top of the H-mode pedestal is observed later in the discharge, when the H-mode is fully formed) are fitted to the L–H transition model prediction from [27, 24]. In this model, the condition for the L–H transition is given by the stabilization of the Alfvén drift wave instability. The coefficients used here for the L–H transition curves are fitted to the JET data, and so they are different from the ones given in [27]. The curve for the predicted L–H temperature boundary at 3.4 T is also shown in the figure. For the 3.4 T data of plasmas with ITB, the predictions of the L–H and Type III models [23, 24] are compared, at low collisionality, with the L-mode data (just before the L–H transition) and ELM free data

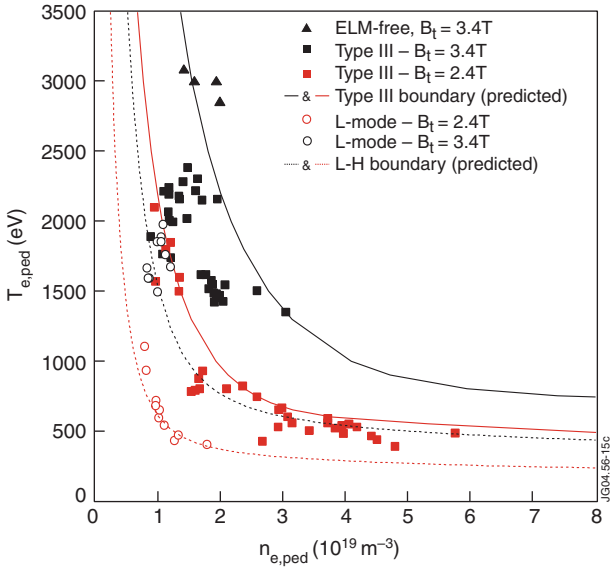

Figure 15. In addition to the set of data of figure 17 and to the predicted T_{0cirt} for Type III ELMs, this figure shows the predicted L–H boundaries for 2.4 and 3.4 T plasmas as well as L–H transition data (○) and data just after the transition from Type III ELMs to the ELM free regime in plasmas with ITBs (▲).

(just after the transition from the Type III to the ELM free regime). A comparison of L–H data with models (see [28]) is outside the scope of this paper: the comparison of the models with the L–H and ELM free data is shown here to illustrate that the combination of these two models predicts the narrow density operational space between the L-mode, Type III ELMs, and Type I ELMs that is found experimentally at low collisionality.

While both in ASDEX-Upgrade and in C-MOD Type III ELMs are found only at high collisionality, Type III ELMs at low density/collisionality were identified also in DIII-D [29]. In DIII-D, Type III ELMs are found in separated collisionality regions of the n_e–T_e space, i.e. no data are found at intermediate collisionality. As pointed out in section 2, the intermediate collisionality region in the n_e–T_e diagram of the 2.4 T JET data is filled by the trajectory of compound ELMs.

The absence of steady state Type III ELMs in this region might be due to the specific experimental conditions since most experiments to study Type III ELMs are carried out either at low densities and powers or at very high densities. Still, the DIII-D observation could suggest that different physics mechanisms could be responsible for Type III ELMs at low and high collisionality. From a comparison of the characteristics of the Type III to Type I transition in standard ELMy H-modes and plasmas with an ITB, current driven peeling modes are indicated in [1] as the candidate instability causing Type III ELMs at low collisionality in plasmas with ITBs. Type III ELMs are observed in ITB plasmas at much higher loss power than the power required to maintain Type I ELMs in standard ELMy H-modes [1, 17]. According to [1], there are strong indications that the main difference between plasmas with and without ITBs could be due to the different current profile and, in particular, to the larger fraction of edge current in ITB plasmas preventing the transition to Type I ELMs. Current driven peeling modes are then stabilized by the increased pressure gradient at higher powers [30]. Although the discussion from [1] might suggest a different physics mechanism for low collisionality Type III ELMs in ELMy H-modes and plasmas with ITBs, experiments where the plasma

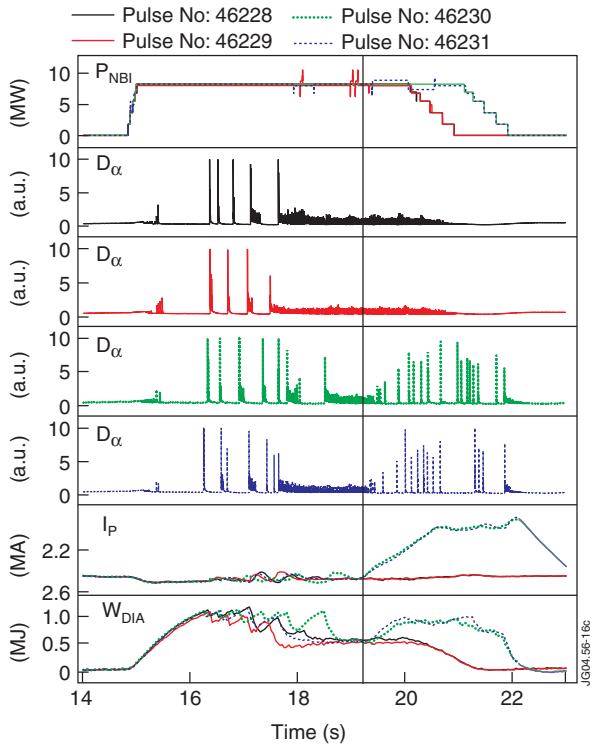

Figure 16. Time traces of the divertor D_α, plasma current, and stored energy for ELMy H-modes with (green and blue traces) and without (black and red traces) I_p ramp-down. In plasmas with input power just below the power required for steady state Type I ELMs, I_p was ramped down during the Type III ELMy phase. The result of the I_p ramp was a transition from Type III to Type I ELMs.

current was ramped down in low collisionality standard Type III ELMy H-modes demonstrate that the edge current might determine the Type I/III ELM transition also in this regime. In figure 16 the time traces with two low density ELMy H-modes without I_p ramp are compared with identical plasmas with an I_p ramp-down from 2.5 to 2 MA during the Type III ELMy phase (with P_{IN} just below P_{TypeI}). Figure 16 shows that, in the discharges where the plasma current was ramped down, a transition from Type III to Type I ELMs was observed. At the transition to Type III ELMs, the local n_e–T_e are consistent with the prediction of the model based on resistive interchange instability. Although the short delay ($<$100 ms), between the start of the I_p ramp and the changes in pedestal and ELM behaviour, suggests an effect only on the plasma edge, an immediate reduction of transport is seen also in the plasma core (figure 17). Experiments where the plasma current was ramped up in an H-mode with Type I ELMs in order to trigger a transition to Type III ELMs did not produce any change in ELM behaviour. This phenomenon might be due to the fact that in those plasmas the additional heating power was much larger than P_{TypeI}. In fact, this result is in contrast with another experiment carried out with the Mark IIA divertor, where an I_p ramp-up produced a transition to L-mode (see section 5), and an I_p ramp-down was observed, inversely, to produce a transition from an L-mode to an H-mode with Type I ELMs [21].

The results of the I_p ramp experiments suggest that it is likely that low density Type III ELMs for plasmas with and without ITBs are driven by the same instability. In addition, as pointed out in section 3, standard ELMy H-modes can have pedestal n_e and T_e values

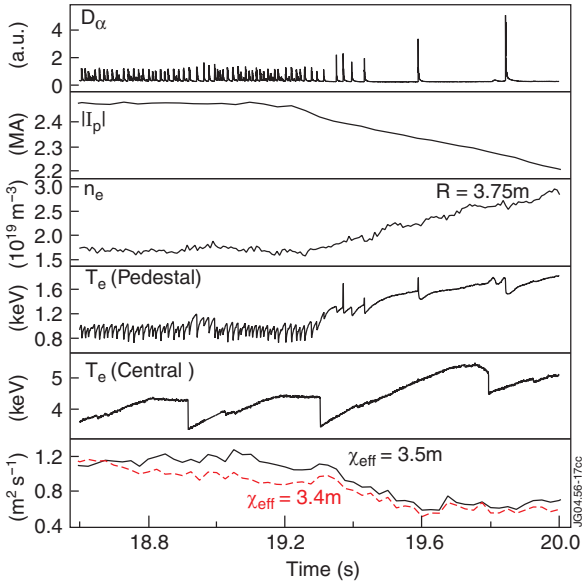

Figure 17. At the transition from Type III to Type I ELMs triggered by the I_p ramp-down, both pedestal density and temperature increase. The increase in the pedestal temperature seen at each sawtooth crash is transient and not sufficient to provoke a transition to Type I ELMs, in the absence of the I_p ramp. At the transition, the transport is reduced also in the plasma core.

in the same region of the pedestal n_e–T_e operational space for ITB plasmas and therefore similar pedestal collisionality. Moreover, the same pedestal temperature boundary at $B_t = 2.4$ and 3.4 T seems to define well the transition from Type III ELMs to Type I ELMs both for plasmas with ITBs (see also [10, 31]) and without ITBs. The changes observed with plasma triangularity are also similar: in both scenarios, a lower power is required for the transition from Type III to Type I ELMs at higher plasma triangularity [19]. Finally, also common to the two regimes is the observation that D–T operation reduces the additional heating power required for the transition to Type I ELMs [9, 10], indicating an inverse mass dependence of P_{TypeI}, and different behaviour of the Mark IIA (L-mode edge) and GB divertor (H-mode edge) [22].

At high densities, the results from JET, ASDEX-U, C-MOD, and DIII-D, show that the transition from Type I to Type III ELMs happens above a critical temperature that is independent of density and increases weakly with toroidal field [24].

In figure 18, the predicted boundary [23, 24] between Type I and Type III ELMs at high densities is shown for the density scans at 8, 11, and 14 MW of input power described in section 7. The L–H predicted boundary [27] is also plotted in the figure to show that the majority of the data for Type III ELMs are found above the predicted L–H boundary.

The JET data suggest that, at high collisionality, the critical temperature for Type III ELMs does not depend strongly on triangularity (see section 7), consistent with the model prediction. In fact, according to the model of Pogutse and Igithkanov, the shear dependence of $T_{0\mathrm{cirt}}$ should be stronger at low collisionality. The variation in the edge shear of the JET low density ELMy H-modes with Type III ELMs is too small to verify the predicted shear dependence of $T_{0\mathrm{cirt}}$, but the variation in critical temperature is consistently small both in the model predictions and in the few data available. Note that the decrease of P_{TypeI}, observed in high triangularity ELMy H-modes both at low and high densities, could also be related to the physics mechanism governing the low pressure boundary of Type I ELMs [32], i.e to the different crashes of temperature and density at the ELM event.

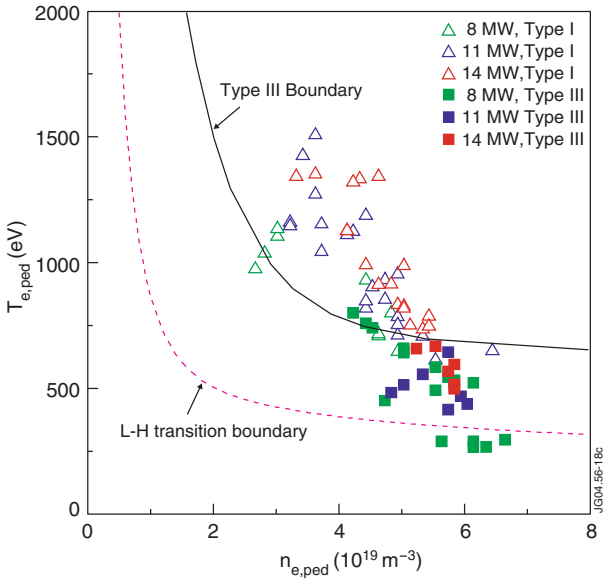

Figure 18. Pedestal n_e–T_e for Type I and Type III ELMs from Mark IIA discharges at 2.5 MA/2.7 T. A density scan was carried out for each level of P_{IN} (8–11 and 14 MW NBI).

The mass dependence predicted by the Pogutse–Igithkanov model was checked against the JET data. The comparison of the data for different isotopes is carried out using the temperature from LIDAR since the ECE data were not available for the hydrogen plasmas. The LIDAR T_e data are taken at a fixed position ($R = 3.75$ m), which is further inside the plasma compared with the typical position of the pedestal. Since the temperature profiles are not as flat as the density profiles, the absolute value of T_e given by LIDAR at 3.75 m is generally higher than the pedestal temperature, so that the data cannot be compared accurately with the model predictions since the fitting coefficients for the model were derived by fitting T_e data from ECE. Even if a quantitative comparison is not possible, figure 19 shows nevertheless that the high density Type III data for different isotopes seem to be separated in density more than in temperature and that the model does not reproduce the trend observed in the experimental data.

Finally, as shown in figure 20, the model of Pogutse–Igithkanov predicts a too strong dependence of the critical temperature on q_{95} for high density JET ELMy H-modes. This wrong dependence of the predicted boundary on q_{95} was also reported, at low collisionality, for plasmas with ITBs [31].

A different model for Type III ELMs at high collisionality describes correctly the q_{95} dependence observed in JET for the transition from Type I to Type III ELMs at high densities. According to the model of Chankin and Saibene [33], Type III ELMs at high densities are driven by resistive ballooning instability, and the dimensionless pressure gradient, $F = q^2 R \Delta\beta / f(s)$ (pressure gradient normalized to the ballooning limit), and collisionality, $v_e^* = Z_{eff} n_e q R / T_e^2$, are the key parameters responsible for the threshold of both ideal and resistive ballooning instabilities. At the transition from Type I to Type III ELMs, while the pedestal temperature (and pressure) always decreases, the pedestal density might either increase or decrease (see also section 7). If the fuelling is increased further with Type III ELMs, an H–L transition is eventually observed. As a consequence, there is a limiting value for the maximum density achievable in an ELMy H-mode. This critical density is given either by the maximum density achievable with Type I ELMs (critical density for the transition to Type III ELMs) or by the

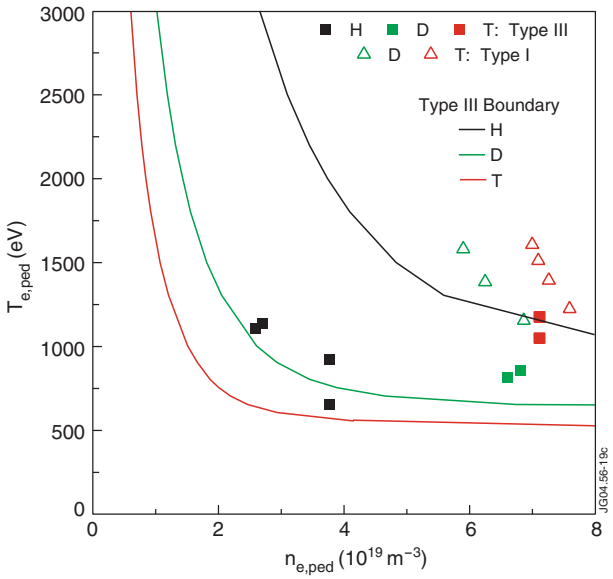

Figure 19. Pedestal n_e–T_e (LIDAR data 3.75 m radius) for gas scans in H, D, and T at 2.5 MA/2.7 T.

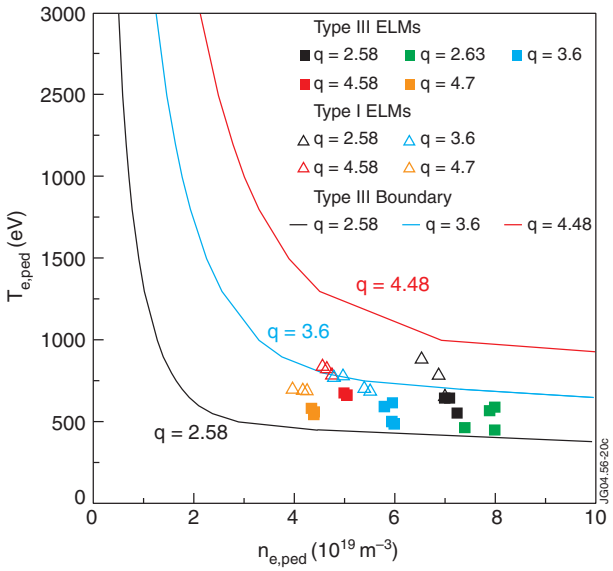

Figure 20. Pedestal n_e–T_e for high density Type I and Type III ELMs in gas scans carried out at different q_{95}. The experimental data in this figure are the same data that were analysed in [7]. q_{95} was varied by varying I_p at constant B_t or B_t at constant I_p in separate gas scans.

density prior to the H–L transition. The H-mode limiting density is usually expressed in terms of the Greenwald density limit, or similar expressions of the form $B^{\alpha}/q^{\beta}R^{\gamma}$. A scaling of the critical density for the transition to Type III ELMs of this form is derived in [33] by fixing the two dimensionless similar parameters, F and ν^*. Experimentally, the density at which the transition from Type I to Type III ELMs is observed in JET is found to scale, at high density, as $n_{e,crit} = B_t/q^{5/4}$. This dependence agrees with the prediction from the model

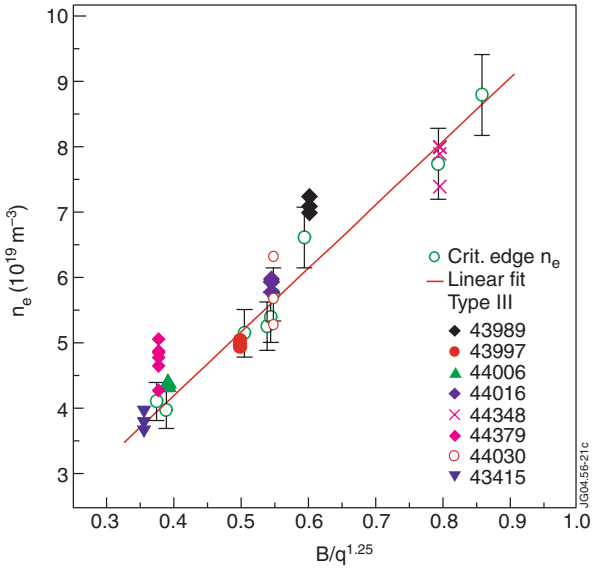

Figure 21. Pedestal density at the Type I–III ELM transition and during Type III ELMs.

$n_{e,crit} \sim B_t f(s)^{1/2}/q^{5/4} R^{3/4} Z_{eff}^{1/4}$. This is shown in figure 21, where n_{ped} data at the transition to high density Type III ELMs are plotted with the scaling curve. The data in the figure are from [11] and from I_p–B_t scans in high density ELMy H-modes with Type III ELMs, at constant plasma shape, P_{IN}, and s_{95}.

In summary, the critical temperature for the stabilization of Type III ELMs predicted by the model of Pogutse and Igithkanov is in good agreement with both the B_t and density dependences of the JET deuterium data at constant q_{95}. Moreover, this model describes well, with a single set of fitting coefficients, the data from different tokamaks. This suggests that the model predicts the correct form of the scaling of T_{crit} in the β, ρ, ν variables.

As noted before, the combination of this model with the L–H transition model predicts the relatively narrow density operational space between L-mode and Type I ELMs, which is observed experimentally in plasmas with ITBs at low collisionality. According to these models, the widest operational space with Type III ELMs (in particular at low collisionality) should be achieved with low magnetic shear and high B_t (as is the case for the ITB plasmas analysed in this paper). In contrast, due to the I_p dependence of the predicted $T_{crit,L–H}$, a high plasma current and high shear should move the L-mode boundary to higher densities and reduce the Type III ELM region, to the extent that the H-mode transition could be directly in the ELM free regime. On the other hand, JET experiments have shown that $T_{crit,L–H}$ does not depend on the plasma current [8].

Discrepancies between the Pogutse–Igithkanov model and experimental data are found regarding the dependence of T_{0crit} on isotopic mass and q. The Chankin–Saibene model predicts the critical density for the transition to Type III ELMs at high collisionality, and the predicted inverse q_{95} dependence is in good agreement with the experimental data. It is difficult, given their different nature, to make a direct comparison between the two models. It is possible, however, that resistive ballooning and interchange instabilities are combined at a high density, where the gap between the ideal ballooning and L–H transition in the n_e–T_e diagram narrows. At low collisionality, the behaviour with I_p ramps and the analysis of ITB plasmas [1] suggest peeling modes as the instability triggering Type III ELMs.

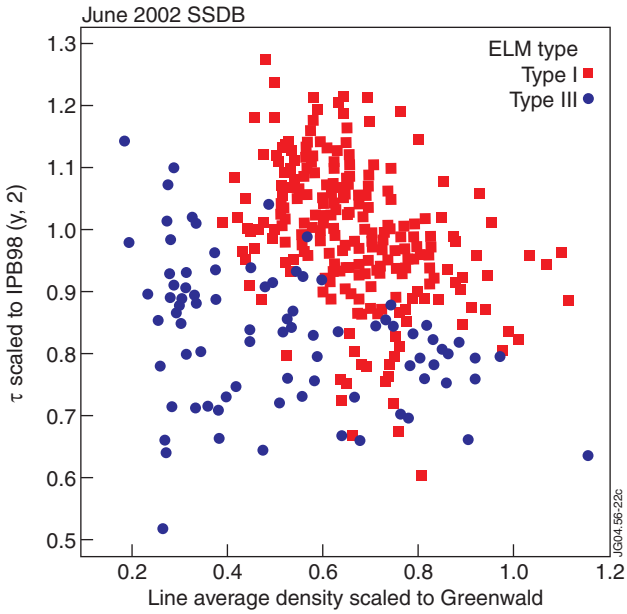

Figure 22. $H98(y, 2)$ versus n_e/n_G for Type I (red) and Type III (blue) ELMy H-modes from the database of steady state ELMy H-modes in JET.

Although it is possible that a different instability is responsible for high and low collisionality Type III ELMs, the JET data also show a continuum in the n_e–T_e operational space that includes data at intermediate collisionality. Moreover, there are common experimental observations for both low and high collisionality Type III ELMs such as the ELM frequency variation with power, the occurrence of these ELMs at low powers above the L–H threshold, and the variation of P_{TypeI} with plasma triangularity as well as the quantitatively similar degradation of the H factor, compared with the Type I ELMs at the same density (see next section).

7. Energy confinement of Type III ELMy H-modes

In JET ELMy H-modes with Type III ELMs, the energy confinement enhancement factor relative to H-mode scaling ($H98(y, 2)$, [34]) is lower than for Type I ELMs, over the entire density range. This is illustrated in figure 22, where the H factor is plotted against the fraction of the core line averaged density over the Greenwald density, for Type I and Type III ELMs. Figure 11 also shows that the H factor of Type III ELMy H-modes degrades with density in a similar way as for Type I ELMy H-modes [11]. The observation that Type III ELMy H-modes with increased triangularity can achieve higher densities with better confinement (see figure 23, from [14] and [35]) is also similar to the Type I ELMy H-mode behaviour. Although data of the energy confinement dependence on triangularity are scarcer for Type III ELMs than for Type I ELMs, the trend shown in figure 23 is confirmed by the data in the JET ELMy H-mode steady state database and holds over the entire density range. As reported in [11], in high density Type III ELMy H-modes, the degradation of confinement (compared to Type I ELMs) is characterized by an enhanced edge cooling and reduced pressure gradient. At the transition, the decrease in pedestal temperature is not compensated by any increase in the pedestal density, resulting in a net loss of pedestal pressure.

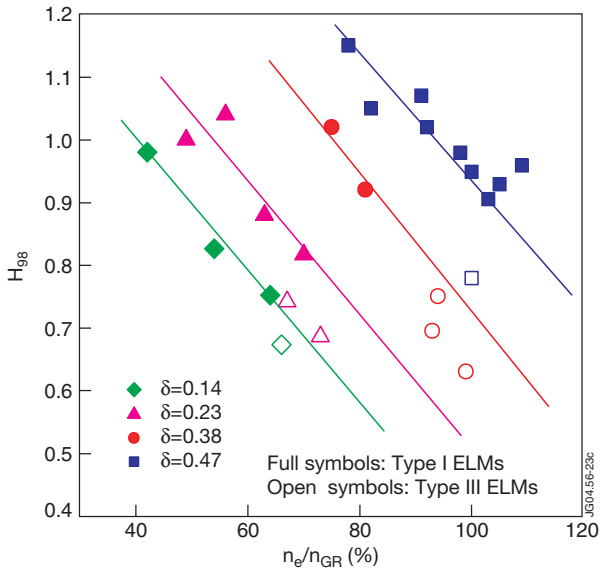

Figure 23. $H98(y, 2)$ versus n_e/n_G for plasmas with different triangularity. The closed symbols are data for Type I ELMy H-modes, and the open symbols are for Type III ELMy H-modes [14].

As reported in [11], the observed decrease in pedestal stored energy at the transition to Type III ELMs at high densities does not account totally for the global confinement losses, and increased core transport also plays a role. In low density ELMy H-modes, the lower plasma pressure is not due to the cooling of the pedestal, as at high densities, but due to lower densities (compared with Type I ELMs) across the plasma profile. The central beam fuelling at low edge n_e values produces slightly more peaked density profiles with Type III ELMs than with Type I ELMs. The central and pedestal T_e values are either unchanged or increased with Type III ELMs compared with Type I ELMs, and $T_i > T_e$. Both the T_e and T_i profiles are more peaked during the low density Type III ELMs than with Type I ELMs.

The pedestal n_e and T_e at the transition from the Type I to the Type III ELMy regime at a high density are shown in figure 24 for 2.5 MA/2.7 T plasmas at different triangularity: $\delta \cong 0.23$ (black symbols), $\delta \cong 0.38$ (red symbols), and $\delta \cong 0.47$ (blue symbols). The density scans at $\delta \cong 0.23$ (with 11 MW NBI), $\delta \cong 0.38$, and $\delta \cong 0.47$ are the same density scans shown in figure 23. In addition, the data from two further density scans with $\delta \cong 0.23$ with 8 and 14 MW NBI are included in figure 24. In this figure, the full symbols represent the n_e–T_e data for the top of the H-mode pedestal in Type I ELMy plasmas (average over the ELM cycle) and the empty symbols are the pedestal data for the Type III ELMy plasmas. The dotted line in the figure divides the Type I ELMy regime from the Type III ELMy regime in terms of pedestal temperature and indicates that, at least at high densities, the critical temperature for the transition to Type III ELMs does not seem to depend on triangularity. Figure 24 also shows that, as the gas fuelling is increased in subsequent discharges with Type III ELMs, the pedestal temperature (and the global confinement, see figure 23) of the Type III ELMy plasmas decreases, as indicated by the arrows in figure 24. While the pedestal T_e always decreases as the fuelling is increased in plasmas with Type III ELMs, the pedestal density responds by either increasing or decreasing. At least for low triangularity plasmas, where the degradation of confinement with density in the Type I ELMy regime is more pronounced than at high δ values, the pedestal pressure degrades continuously from the Type I to Type III ELMy regimes, with

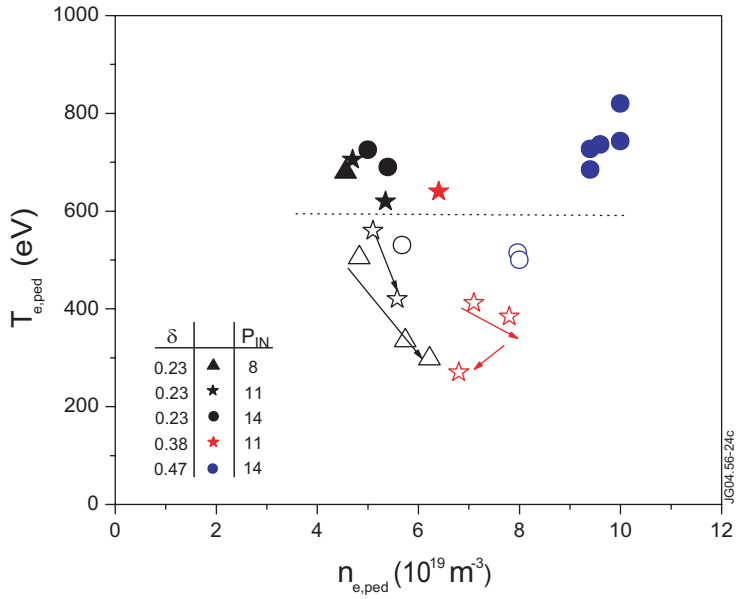

Figure 24. Pedestal T_e versus pedestal n_e for Type I and Type III ELMy plasmas at high densities. Empty symbols, Type III ELMs; full symbols, Type I ELMs.

the Type I ELMy plasmas at the highest density and the Type III ELMy plasmas having very similar pedestal pressure and confinement.

The plasma with $\delta \cong 0.47$ in figure 24 has a behaviour different from those at lower δ values at the transition from Type I to Type III ELMs: a large decrease in the pedestal n_e is observed as well as a drop in the pedestal T_e. It is not clear what causes this loss of pedestal n_e, or if the correlation between the different behaviour of the pedestal n_e at the transition to Type III ELMs and the plasma δ, which is suggested by the data in figure 24, is indeed an effect of triangularity. In fact, a decrease in pedestal density at the transition to Type III ELMs is sometimes observed also at low δ values (see also [11]).

8. Summary and conclusions

The Type III ELMy regime in JET is found in a large operational space in terms of the pedestal n_e–T_e, with Type III ELMs being observed in standard ELMy H-modes as well as in plasmas with an ITB. Steady state Type I ELMy H-modes are only observed above a critical power, P_{TypeI}. At powers just below P_{TypeI}, the plasma can access the Type I ELM regime and sometimes maintain it for several energy confinement times, but cyclic or permanent transitions to Type III ELMs are then observed. In JET, for a given plasma triangularity, P_{TypeI} is proportional to the L–H threshold power and decreases for increasing δ. P_{TypeI} is also observed to increase at low densities. The highest P_{TypeI} is for a low density low triangularity ($\delta \cong 0.25$) plasma where the Type I ELMy regime and the good confinement associated with it can be maintained in a steady state with a power of about twice the L–H threshold power. A reduction in P_{TypeI} of 20–30% is observed for an increase in δ from $\cong$0.2 to $\cong$0.3.

In the pedestal n_e–T_e diagram, the density of JET plasmas with Type III ELMs can be as low as 20% of the Greenwald limit, n_G, or as high as $\cong n_G$. The critical pedestal temperature for the transition from Type III to Type I ELMs, T_{cirt}, increases with decreasing density ($T_e \propto 1/n_e$)

at low a density and is approximately constant at high density. At low densities, $T_{\rm cirt}$ increases with toroidal field ($T_{\rm e} \propto B_{\rm t}^2$) at constant q_{95}.

Plasmas with an ITB and Type III ELMy edge have generally lower pedestal $n_{\rm e}$ and higher pedestal $T_{\rm e}$ values than standard ELMy H-modes. Nevertheless, with a similar plasma configuration optimized for divertor pumping, the $n_{\rm e}$–$T_{\rm e}$ of low density Type III ELMy H-modes overlaps with the operational range of plasmas with an ITB. Similar to what is observed in standard ELMy H-modes, an increase in density at constant power can trigger a transition to Type I ELMs also in Type III ELMy plasmas with ITBs [10]. Also similar for the two regimes is the observed reduction in the power required to access the Type I ELMy regime with increasing triangularity [19] and isotopic mass. The similarities in the pedestal behaviour of plasmas with and without an ITB indicate that the ELMs are driven by the same instability, despite the fact that only for standard ELMy H-modes has it been proven in JET that the ELM frequency follows the inverse power dependence, typical of Type III ELMs. The most significant difference between the two regimes is the much higher power at which Type III ELMs are still observed in plasmas with ITBs. This difference cannot be explained only in terms of the decrease in $P_{\rm TypeI}$ with decreasing density [1]. All the above results are common to the JET Mark IIA and GB divertors. Only one significant difference between the two divertors was observed in low collisionality plasmas with and without ITBs: at powers below $P_{\rm TypeI}$, the Mark IIA plasma remained in L-mode. This difference is attributed to the presence of an additional $n = 1$ low frequency pedestal instability in the MARK IIA plasmas, which prevented them from maintaining an H-mode pedestal with Type III ELMs. This instability, of unknown nature, was stabilized for $P > P_{\rm TypeI}$.

The JET data, in contrast with results from other tokamaks, indicate that the operational space for Type III ELMs covers a wide range of pedestal collisionality. The common observations at low and high collisionalities are the ELM frequency dependence on power, the occurrence of Type III ELMs at low powers above the L–H threshold power, the effect of plasma triangularity and isotopic mass, and, not discussed in this paper, the fact that, the ELM crash is smaller than for Type I ELMs in the entire collisionality range [35]. These common observations are indicative of a common physics mechanism for the ELM trigger.

A model for Type III ELMs (Pogutse–Igithkanov [23, 24]) that considers the resistive interchange instability with magnetic flutter was tested against the JET experimental data. The model predicts well, over the entire collisionality range, the density dependence of the critical temperature for the transition to Type I ELMs in JET as well as in other tokamaks. In JET, this model also predicts the experimentally observed toroidal field dependence of the critical temperature of Type III ELMs. Nevertheless, the JET results show that such a model does not describe correctly the experimental variation of the critical temperature with isotopic mass and with q_{95}. Other experimental observations suggest instead that a different instability might be responsible for Type III ELMs at different collisionality. At low collisionality, in plasmas with and without an ITB, a current ramp-down triggers the transition from Type III to Type I ELMs, indicating a role of the edge currents and suggesting current driven peeling modes as the candidate instability. At high collisionality, a model (Chankin–Saibene [33]) based on the resistive ballooning instability reproduces correctly the JET data for the transition from Type I to Type III ELMs in terms of the critical density, $n_{\rm e,crit} = B_{\rm t}/q^{5/4}$.

In JET Type III ELMy H-modes, the energy confinement enhancement factor degrades with density and increases with triangularity over the entire collisionality range in a manner similar to that for H-modes with Type I ELMs, indicating that these two trends are not specifically related to the ELM type. Although the reduction in confinement with Type III ELMs with respect to Type I ELMy H-modes is quantitatively similar at high and low densities, the signatures are different. In fact, while at high densities the degradation of confinement is

mainly due to the cooling of the pedestal (sometimes accompanied by loss of pedestal density), at low densities the pedestal temperature does not vary or increases at the transition from Type I to Type III ELMs, and the loss of pedestal pressure is mainly caused by a strong decrease in the pedestal density. Similar to what is observed with Type I ELMs, a higher density with better global confinement is achieved also in the Type III ELMy regime by increasing the plasma triangularity. Nevertheless, the few data available suggest that, at least at a high density, the relative degradation of confinement at the transition from Type I to Type III ELMs might be more substantial at higher δ values, mainly due to the larger loss of pedestal density at the transition.

Acknowledgments

The authors would like to acknowledge the contribution of the JET Joint Undertaking JET Team to the work presented in this paper.

References

[1] Sarazin Y *et al* 2002 *Plasma Phys. Control. Fusion* **44** 2445
[2] Campbell D J 2001 *Phys. Plasmas* **8** 2041
[3] Horton L D *et al* 1999 *Nucl. Fusion* **39** 993
[4] ITER Confinement Database and Modelling Expert Group (presented by Takizuka T) 1996 *Fusion Energy* vol II p 795 IAEA-CN64/F-5
[5] Doyle E J *et al* 1991 *Phys. Fluids* B 3
[6] Zohm H 1996 *Plasma Phys. Control. Fusion* **38** 105
[7] Sartori R *et al* 1999 *Proc. 26th EPS on Controlled Fusion and Plasma Physics* vol 23J (Geneva: EPS) p 197
[8] Horton L D *et al* 1999 *Proc. 26th EPS on Controlled Fusion and Plasma Physics* vol 23J (Geneva: EPS) p 193
[9] Righi E *et al* 1999 *Nucl. Fusion* **39** 309
[10] JET Team (prepared by ACC Sips) 2001 *Nucl. Fusion* **41** 1559
[11] Saibene G *et al* 1999 *Nucl. Fusion* **39** 1133
[12] Sartori R *et al JET Report* R(00) 01
[13] Sartori R *et al* 2002 *Plasma Phys. Control. Fusion* **44** 1801
[14] Saibene G *et al* 2002 *Plasma Phys. Control. Fusion* **44** 1769
[15] Suttrop W *et al* 1997 *Plasma Phys. Control. Fusion* **39** 2051
[16] Soeldner F X *et al* 1997 *Plasma Phys. Control. Fusion* **39** B 353
[17] Becoulet M *et al* 2002 *Plasma Phys. Control. Fusion* **44** A103
[18] The JET Team (presented by Righi E) 2000 *Proc. 18th Int. Conf. (Sorrento)* IAEA-CN-77
[19] Lomas P J *et al* 2001 *Proc. 9th European Fusion Physics Workshop (Saariselka, Finland, December 2001)*
[20] Horton L D *et al* 1999 *Nucl. Fusion* **39** 1
[21] Sartori R *et al* 1998 *Plasma Phys. Control. Fusion* **40** 757
[22] Gormezano C *et al* 1999 *Plasma Phys. Control. Fusion* **41** 367
[23] Pogutse O *et al Proc. 26th EPS on Controlled Fusion and Plasma Physics* vol 23J, p 249
[24] Igitkhanov Yu and Pogutse O 2000 *Contrib. Plasma Phys.* **40** 368
[25] Suttrop W 1999 *Plasma Phys. Control. Fusion* **42** A1
[26] Horton L D *et al* 1999 *Plasma Phys. Control. Fusion* **41** B329
[27] Pogutse O and Igitkhanov Yu 1997 *Proc. 24th European Conf. Berchtesgaden* vol 21A (Part III) p 1041
[28] The ITER H-mode Threshold Database Working Group (presented by Righi E) 1998 *Plasma Phys. Control. Fusion* **40** 857
[29] Osborne T H *et al* 1997 *Proc. 24th EPS on Controlled Fusion and Plasma Physics* vol 21A (Part III) (Geneva: EPS) p 1101
[30] Snyder P B *et al* 2002 *Phys. Plasmas* **9** 2037
[31] Becoulet M *et al* 2001 *Proc. 28th European Conf. (Funchal)* vol 25A, p 1605
[32] Loarte A *et al* 2002 *Plasma Phys. Control. Fusion* **44** 1815
[33] Chankin A and Saibene G 1999 *Plasma Phys. Control. Fusion* **41** 913
[34] Cordey J G *et al* 1997 *Plasma Phys. Control. Fusion* **39** B115
[35] Rapp J *et al* 2002 *Plasma Phys. Control. Fusion* **44** 639